One-step fabrication and high photocatalytic activity of porous graphitic carbon nitride synthesised via direct polymerisation of dicyandiamide without templates

Qingbo Yu[1], *Xianhua Li*[2], *Mingxu Zhang*[1]

[1]*Department of Materials Science and Engineering, Anhui University of Science and Technology, Huainan 232001, People's Republic of China*
[2]*School of Mechanical Engineering, Anhui University of Science and Technology, Huainan 232001, People's Republic of China*
E-mail: xhli01@163.com

Published in Micro & Nano Letters; Received on 4th November 2013; Accepted on 22nd November 2013

Porous graphitic carbon nitride (g-C_3N_4) has been synthesised by means of one-step calcinations of dicyandiamide for efficient photocatalysis under visible light irradiation ($\lambda > 400$ nm). Scanning electron microscopy images demonstrate that the as-prepared photocatalyst calcined at 650°C is a porous structure. The UV–vis diffuse reflectance spectra show that the optical absorption for the porous g-C_3N_4 is more intensive than for common g-C_3N_4 calcined at 550°C. The enhanced generation of the photocurrent under visible light irradiation ($\lambda > 400$ nm) is observed by using the porous g-C_3N_4. The results of the photocatalytic experiments under visible light irradiation reveal that the photocatalytic degradation of methylene blue using the porous g-C_3N_4 is higher than common g-C_3N_4, showing the advantage of the structure for efficient photocatalysis. The presence of the calcinations temperature is presumed to play a key role in adjusting the textural properties.

1. Introduction: Recently, an organic, graphitic carbon nitride (g-C_3N_4), composed of C and N elements only, has demonstrated great potential in metal-free photocatalyst for the elimination of pollutants [1]. However, the efficiency for the first generation of g-C_3N_4 is rather low. To enhance the photocatalytic ability, various nanomorphologies or dopings have been prepared by means of chemical or physical methods [2].

Porous structure materials are especially attractive because they can enhance the efficiency of energy conversion by increasing the semiconductor surface area and creating multiple scattering effects [3]. The first mesoporous g-C_3N_4 is obtained by nanocasting/replication of mesoporous silica matrices, which are well-known from the generation of the corresponding carbon nanostructures [4–6]. Other strategies involve the use of ethylenediamine (EDA) and carbon tetrachloride (CTC) as precursors [7–9]. For example, Vinu *et al.* reported the synthesis of mesoporous g-C_3N_4 by nanocasting techniques through a simple polymerisation reaction between CTC and EDA. The use of the surfactants and the block polymers as 'soft templates' for the production of mesoporous g-C_3N_4 is another important method. It can be successfully synthesised by introducing holding sequences in the heating program according to the decomposition temperature of the surfactants [10]. However, most of these systems require additional hard templates and/or complicated post-treatments. Thus, it is highly desirable to develop a simple, template-free and direct strategy to improve the reactivity of primitive g-C_3N_4.

Gas bubbles produced during reaction have been frequently used as soft templates to help inorganic nanocrystals form porous microstructures [11]. Compared with the other template-synthetic methods, this soft-template method is very simple, convenient and avoids the introduction of impurities, and is therefore suitable for the synthesis of porous microstructures. Also, Thomas *et al.* [12] described the synthesis of condensed carbon nitrides. The precursors are first condensing towards melamine. The second step is a condensation where ammonia is eliminated. In addition, Lotsch and Schnick [13] probed the identity of the species evolved in the processing of carbon nitride condensation by temperature-dependent gas-phase vibrational spectroscopy. As observed, strong absorption because of ammonia emerges about 470 K and grows continuously up to the end of the measurements at 740 K.

Here, we report a convenient approach to obtaining porous g-C_3N_4 from dicyandiamide with self-supported gas and study its photocatalytic activity.

2. Experimental

2.1. Materials: All of the reagents (analytical grade purity) were purchased from the Tianjin Kermel Chemical Reagents Development Centre and were used without further purification. ITO glass was purchased from Geao Co., China.

2.2. Preparation of g-C_3N_4: The photocatalyst of g-C_3N_4 was prepared by directly heating dicyandiamide. A quartz boat loaded with dicyandiamide was placed into the centre of a tube furnace. Pure argon was introduced into the quartz tube at a flow rate of 200 sccm (standard cubic metre per minute) for 30 min before the flow rate was decreased to 50 sccm; the pressure inside the tube was held constant at 1 atm. The furnace was gradually heated to 450°C at a rate of 3 K min^{-1} and held at this temperature for 4 h. After cooling the tube furnace to room temperature a faint product was found. The further heating treatment was performed at 550 and 650°C for 4 h, respectively. We found that after the dicyandiamide was held at 750°C for 4 h, there was no residual carbon left in the quartz boat.

2.3. Photocatalytic experiment: Photocatalytic activity of g-C_3N_4 for methylene blue (MB) photodegradation was evaluated in a Pyrex reactor. 0.3 g of g-C_3N_4 was dispersed in MB aqueous solution (100 ml and 0.2 mgl^{-1}). The light irradiation system contains a 300WXe lamp with a cutoff filter for visible light and a water filter to eliminate the temperature effect. The intensity of the corresponding incident light is 1.2 mW/cm^2. Radiometers of model FZ-A (Photoelectric Instrument Factory Beijing Normal University) were used to measure the incident visible light intensity. The recycle experiments were performed. After filtering the sedimentation of the photocatalyst by a vacuum filter, the obtained photocatalyst was redispersed in 100 ml MB solution.

The adsorption and the photocatalytic process were the same with the above-mentioned one.

2.4. Characterisation: The samples were characterised by X-ray diffraction (XRD) for phase identification on the Rigaku RINT2000 diffractometer. UV–vis diffuse reflection spectra were measured by using a UV–vis spectrophotometer (Varian CARY 100, USA) and converted from reflection to absorbance by the Kubelka-Munk method. The morphology of the product was analysed by scanning electron microscopy (SEM). The structural information of the samples was measured by a Fourier transform spectrophotometer (FTIR). The photocurrent measurements, using 2 M sodium sulphate as electrolyte, were performed in a standard three-electrode cell, which used an Ag/AgCl electrode as the reference electrode and a Pt plate as the counter electrode. The g-C_3N_4 on indium-tin oxide (ITO) coated glasses were used as the working electrode. They were connected to a CHI electrochemical analyser (CH Instruments 650 B, Shanghai Chenhua). A high pressure xenon short arc lamp (CHF-XM35-500 W, Beijing Changtuo) provided full spectrum illumination; a filter was used to allow visible light ($\lambda > 400$ nm) to pass through. The specific surface area was determined with the Brunauer-Emmett-Teller (BET) equation at 77 K by using an adsorption apparatus (Micromeritics ASAP2020M +C).

3. Results and discussion: XRD patterns, SEM images and FTIR spectrum are used to investigate the structure of the prepared samples. The SEM images are shown in Figs. 1*a–c*. The sample calcined at 450°C is composed of a floccules-wrapped rod-like structure (Fig. 1*a*). When the temperature is increased to 550°C, a crumb structure consisting of sheets is obtained (Fig. 1*b*). It should be noted that a typical porous morphology in each sheet is exhibited when the calcination temperature reaches 650°C (Fig. 1*c*). The specific surface area of the porous g-C_3N_4 is investigated by using nitrogen adsorption and desorption isotherms (the inset of Fig. 1*c*). The BET specific surface area of the sample is calculated from the N_2 isotherms at 77 K and is found to be 45.6 m^2/g.

The typical XRD patterns of the samples are shown in Fig. 1*d*. A series of diffraction peaks may be discerned for curve 1 in the 2θ range between 10° and 35°. In fact, the XRD pattern illustrated by curve 1 resembles to a large extent that of the crystalline powders of melem, which has been indexed with a monoclinic unit cell [14]. Thus, it can be implied that the sample obtained by 450°C may yield a melem-like molecular solid. However, the situations are quite different when the temperatures are raised. As for curves 2 and 3 in Fig. 1*d*, the strongest XRD peak (002) at around 27.4° ($d = 0.325$ nm) is a characteristic inter-planar stacking peak of conjugated aromatic systems. Another distinct peak (100) at 13.1° ($d = 0.675$ nm) can be attributed to an in-planar structural packing motif. They confirm a graphitic-like layer structure for the sample calcined at 550 and 650°C [15].

The typical FTIR spectra of the prepared samples are displayed in Fig. 2. As for Fig. 2*a*, a broad but structured absorption band in the region between 800 and 1700 cm^{-1} dominates the spectrum, with distinguishable maxima at 804, 887, 1089, 1258, 1330, 1464 and 1609 cm^{-1}. The well-resolved bands may indicate a fairly high degree of ordering, which is in accordance with our XRD

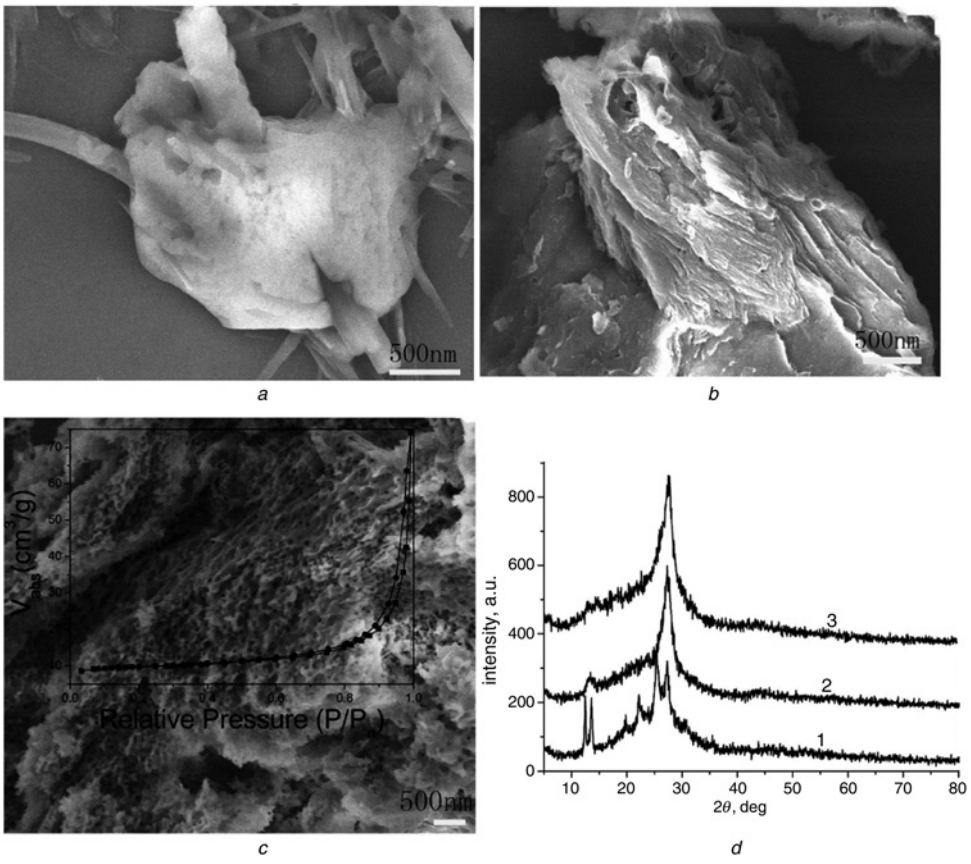

Figure 1 *Typical SEM images*
a 450°C
b 550°C
c 650°C and
XRD patterns
d 1: 450°C; 2: 550°C and 3: 650°C) of the samples fabricated from different temperatures
Inset in Fig. 1*c* are the N_2 adsorption and desorption isotherms

doi: 10.1049/mnl.2013.0651

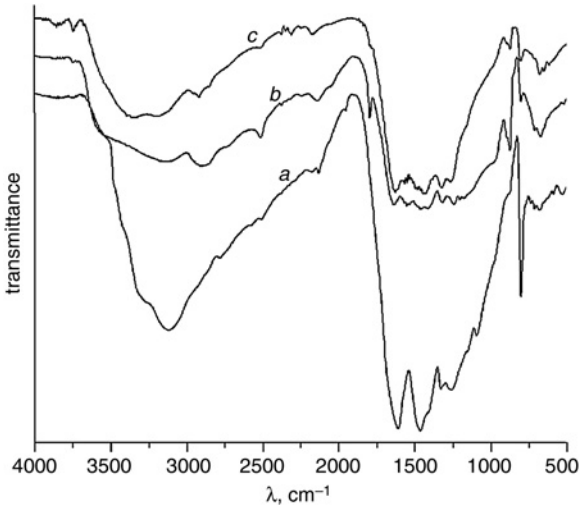

Figure 2 *FTIR spectra for the samples fabricated from different temperatures: a 450°C, b 550°C and c 650°C*

investigations. Owing to obvious analogies with the vibrational spectra of the heptazine compounds already present in the literature, such as those of $C_6N_7C_{l3}$, $C_6N_7(N_3)_3$ and $C_6N_7(NH_2)_3$ [16], the observed absorptions may be readily assigned to the skeletal vibration modes belonging to the C_6N_7 nucleus.

As for Figs. 2*b* and *c*, the FTIR spectrum also suggests the existence of a graphite-like sp^2 bonded structure. The absorption band near 1630 cm^{-1} is attributed to C = N stretching [17], whereas the three at 1249, 1320 and 1427 cm^{-1} to aromatic C–N stretching. The peak at 807 cm^{-1} belongs to the triazine ring modes, which correspond to the condensed CN heterocycles [18]. The above result confirms the formation of the g-C_3N_4 when the heat treatment temperature changed from 550 to 650°C. Hence, the two samples are investigated in the following.

To study the optical response of the as-prepared samples, their UV–vis absorption spectra are measured, and the results are shown in Fig. 3. We can see that the absorption edges of the samples obtained from heating dicyandiamide shift remarkably to longer wavelengths with increasing heating temperature. The decrease in the bandgaps of the samples is from 2.63 to 2.34 eV when the heat treatment temperature is increased from 550 to 650°C. The spectra of the samples heated at higher temperature, 650°C, show an absorption tail. This probably is attributed to the

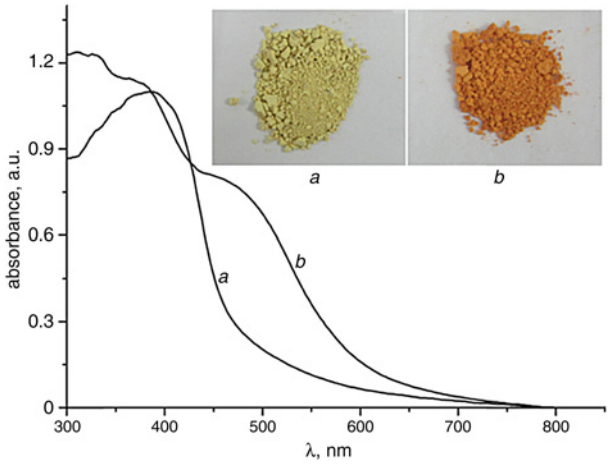

Figure 3 *UV–vis absorption spectra for the g-C_3N_4 samples obtained by different temperatures*
Insets are the colour evolution of the g-C_3N_4 samples): *a* 550°C and *b* 650°C

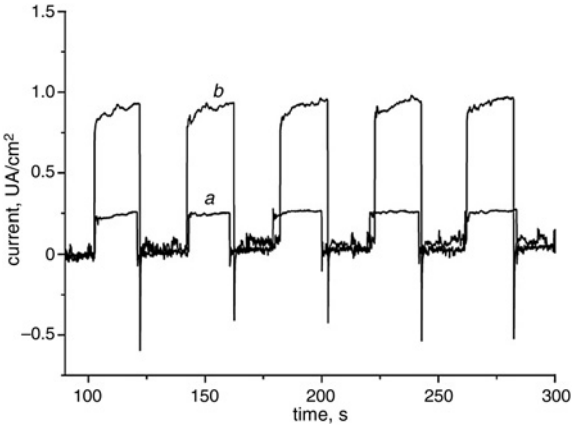

Figure 4 *Photocurrent densities of the g-C_3N_4 samples obtained by different temperatures (a 550°C and b 650°C) under visible light irradiation ($\lambda > 400$ nm)*

porous structure formed in the samples treated at high temperatures, which improve the optical absorption of the materials [19]. In addition, the colours display evolution from yellow to red when the heat treatment temperature is increased, which also implies that the intrinsic optical properties have changed.

Fig. 4 shows the photocurrent densities of the g-C_3N_4 samples obtained by different temperatures under visible light illumination ($\lambda > 400$ nm). When the temperature is 550°C, the photocurrent is low under visible light irradiation. When the temperature is increased to 650°C, the photocurrent is 3.72 times as great as that of the common g-C_3N_4 samples obtained by 550°C under visible light irradiation. This enhancement resulted from the increased visible absorption owing to the porous structure, which led to the increase of the photogenerated carriers. This experiment confirms that porous g-C_3N_4 possesses enhanced photoresponse than common g-C_3N_4.

The photocatalytic activities of the samples prepared at different temperatures were evaluated for MB photodegradation under visible light ($\lambda > 400$ nm) irradiation, as shown in Fig. 5. For comparison, an experiment with a commercial TiO_2 sample was also performed under the same conditions. The initial MB concentration affects degradation efficiency. Song *et al.* [20] indicated that the MB degradation efficiency decreased with increased initial MB concentration. Hence, we chose an initial MB concentration of 0.2 mg l^{-1}. From Fig. 5*a*, without any catalyst, the MB decomposition rate is only about 5%, which can be accounted for by the natural photodegradation of the MB molecules. It is obvious that the photocatalytic activities for all the g-C_3N_4 samples are much higher than those of the TiO_2. We can find out that the main absorption edge of TiO_2 is at 390 nm in the UV–vis absorption spectra [21]. The weak light absorption of TiO_2 in the visible region means poor visible light response. As a result, TiO_2 has a low activity for photodegrading MB. The g-C_3N_4 sample obtained at 650°C disappeared not only under stronger adsorption of MB on the catalyst surface but also more rapidly under photodegradation of the MB than the common g-C_3N_4 samples obtained by 550°C. The high adsorption for the MB may be ascribed to two reasons: firstly, the porous structure produced from the high calcinations temperature causes large adsorption capacity, with almost 77% MB adsorbed on the porous g-C_3N_4, secondly, the g-C_3N_4 material itself has good adsorption capacity for MB. Di *et al.* [22] evaluated the isoelectric point of the g-C_3N_4 by the zeta-potential measurements. It was found to be approximately pH 4.1, which was not unexpected because the g-C_3N_4 could easily adsorb cationic dye (MB). Moreover, the high photocatalytic activity of the porous g-C_3N_4 is probably because of dye-sensitisation caused by stronger adsorption of the MB. Moon *et al.* [23] indicate that the adsorption

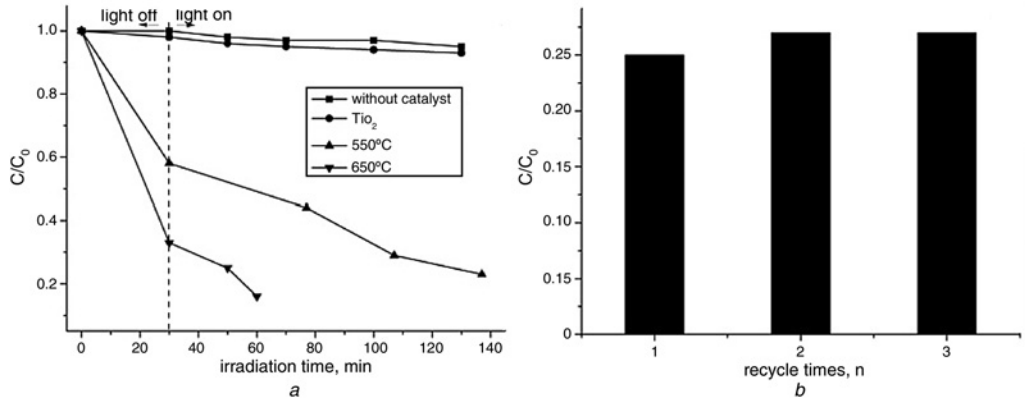

Figure 5 *Photodegradation of methyl orange*
a Over the commercial TiO_2 and the g-C_3N_4 obtained by heating at different temperatures
b Recycle test

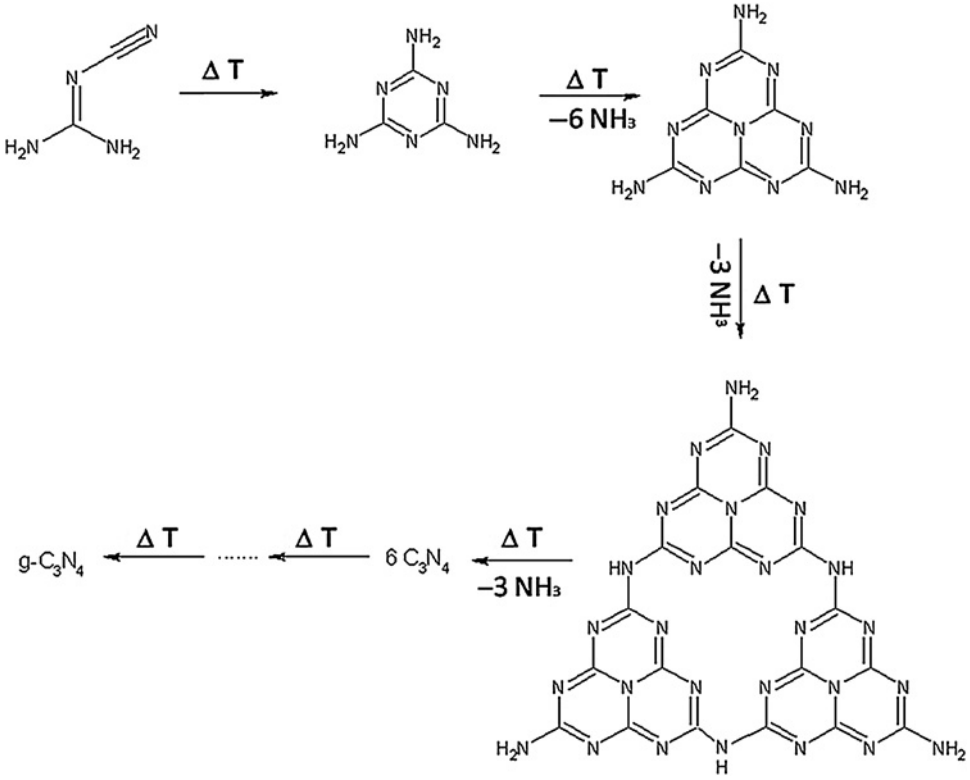

Figure 6 *Microscopic mechanism of the reaction paths of g-C_3N_4*

of the dye is an important factor in dye-photosensitisation, which can enhance photodegradation under visible light. It is necessary to measure the recyclability of the g-C_3N_4 as an efficient photocatalyst. Fig. 5*b* shows that the photocatalytic activity is stable with the MB in solution decomposed during the 20 min irradiation for each cycle, although a small decline (<3%) can be detected after three cycles.

Finally, to understand the advantages of the calcinations temperature, the microscopic mechanism of the reaction paths of the g-C_3N_4 may be sketched as shown in Fig. 6 on the basis of the above discussion, along with the former experimental studies [12, 13] and the ab initio calculations [24].

As usual, dicyanamide is recommended to be used as a precursor and promotes a rather rapid passage of the melamine phase to increase the mass efficiency in the polymerisation process. The dicyanamide precursor undergoes a polyaddition process to form the g-C_3N_4, they release NH_3 when there is a thermal polymerisation process. The gas bubbles favour the formation of a porous structure. In consideration of the distinctly different porous properties, the effect of the calcinations temperature must be taken into consideration. On the one hand, the high calcinations temperature is favourable for high polymerisation of the g-C_3N_4, which will increase the quantity of NH_3 [25].

On the other hand, the high calcinations temperature increases the rate of NH_3, which leads to numerous gas bubbles in a short time. As a whole, although the self-generated NH_3 exists in the other calcinations temperature, the high calcinations temperature obviously favours a more condensed and porous product, in accordance with our experimental results.

4. Conclusion: In summary, we have explored porous g-C_3N_4 simply polymerised from dicyandiamide in argon with

doi: 10.1049/mnl.2013.0651

semiconductor characteristics without extra templates. The porous g-C_3N_4 exhibits higher photocatalytic activity than common g-C_3N_4. Thus, it is worth further developing porous g-C_3N_4 with inexpensive, active dicyandiamide.

5 References

[1] Wang X., Maeda K., Thomas A., *ET AL.*: 'A metal-free polymeric photocatalyst for hydrogen production from water under visible light', *Nat. Mater.*, 2009, **8**, pp. 76–80

[2] Wang Y., Wang X., Antonietti M.: 'Polymeric graphitic carbon nitride as a heterogeneous organocatalyst: from photochemistry to multipurpose catalysis to sustainable chemistry', *Angew. Chem. Int. Ed.*, 2012, **51**, pp. 68–89

[3] Soler-lllia G.L.A.A., Sanchez C., Lebeau B., Patarin J.: 'Chemical strategies to design textured materials: from microporous and mesoporous oxides to nanonetworks and hierarchical structures', *Chem. Rev.*, 2002, **102**, pp. 4093–4138

[4] Groenewolt M., Antonietti M.: 'Synthesis of g-C_3N_4 nanoparticles in mesoporous silica host matrices', *Adv. Mater.*, 2005, **17**, pp. 1789–1792

[5] Liang C.D., Hong K.L., Guiochon G.A., Mays J.W., Dai S.: 'Synthesis of a large-sale highly ordered porous carbon film by self-assembly of block copolymers', *Angew. Chem.*, 2004, **116**, pp. 5909–5913

[6] Thomas A., Goettmann F., Antonietti M.: 'Hard templates for soft materials: creating nanostructured organic materials', *Chem. Mater.*, 2008, **20**, pp. 738–755

[7] Vinu A., Ariga K., Mori T., *ET AL.*: 'Preparation and characterization of well-ordered hexagonal mesoporous carbon nitride', *Adv. Mater.*, 2005, **17**, pp. 1648–1652

[8] Jin X., Balasubramanian V.V., Selvan S.T., *ET AL.*: 'Highly ordered mesoporous carbon nitride nanoparticles with high nitrogen content: a metal-free basic catalyst', *Angew. Chem.*, 2009, **121**, pp. 8024–8027

[9] Srinivasu P., Vinu A., Hishita S., Sasaki T., Ariga K., Mori T.: 'Preparation and characterization of novel microporous carbon nitride with very high surface area via nanocasting technique', *Microporous Mesoporous Mater.*, 2008, **108**, pp. 340–344

[10] Wang Y., Wang X.C., Antonietti M., Zhang Y.J.: 'Facile one-pot synthesis of nanoporous carbon nitride solids by using soft templates', *ChemSusChem*, 2010, **3**, pp. 435–439

[11] Peng Q., Dong Y.J., Li Y.D.: 'ZnSe semiconductor hollow microspheres, Angew', *Chem., Int. Ed.*, 2003, **42**, pp. 3027–3030

[12] Thomas A., Fischer A., Goettmann F., *ET AL.*: 'Graphitic carbon nitride materials: variation of structure and morphology and their use as metal-free catalysts', *J. Mater. Chem.*, 2008, **18**, pp. 4893–4908

[13] Lotsch B.V., Schnick W.: 'Thermal conversion of guanylurea dicyanamide into graphitic carbon nitride via prototype CNx precursors', *Chem. Mater.*, 2005, **17**, pp. 3976–3982

[14] Jürgens B., Irran E., Senker J., Kroll P., Müller H., Schnick W.: 'Melem (2,5,8-Triamino-tri-s-triazine), an important intermediate during condensation of melamine rings to graphitic carbon nitride: synthesis, structure determination by X-ray powder diffractometry, solid-state NMR, and theoretical studies', *J. Am. Chem. Soc.*, 2003, **125**, pp. 10288–10300

[15] Wang X., Maeda K., Thomas A., *ET AL.*: 'A metal-free polymeric photocatalyst for hydrogen production from water under visible light', *Nat. Mater.*, 2008, **8**, pp. 76–80

[16] Kroke E., Schwarz M., Horath-Bordon E., Kroll P., Noll B., Norman A.D.: 'Tri-s-triazine derivatives. Part I: From trichloro-tri-s-triazine to graphitic C_3N_4 structures', *New J. Chem.*, 2002, **26**, pp. 508–512

[17] Bousetta A., Lu M., Bensaoula A., Schultz A.: 'Formation of carbon nitride films on Si (100) substrates by electron cyclotron resonance plasma assisted vapor deposition', *Appl. Phys. Lett.*, 1994, **65**, pp. 696–698

[18] Khabashesku V.N., Zimmerman J.L., Margrave J.L.: 'Powder synthesis and characterization of amorphous carbon nitride', *Chem. Mater.*, 2000, **12**, pp. 3264–3270

[19] Zhao Y., Yang B., Xu J., Fu Z., Wu M., Li F.: 'Facile synthesis of Ag nanoparticles supported on TiO_2 inverse opal with enhanced visible-light photocatalytic activity', *Thin Solid Films*, 2012, **520**, pp. 3515–3522

[20] Song L., Zhang S., Wu X., Wei Q.: 'A metal-free and graphitic carbon nitride sonocatalyst with high sonocatalytic activity for degradation methylene blue', *Chem. Eng. Process.*, 2012, **184**, pp. 256–260

[21] Rajeshwar K., de Tacconi N.R., Chenthamarakshan C.R.: 'Semiconductor-based composite materials: preparation, properties, and performance', *Chem. Mater.*, 2001, **13**, pp. 2765–2782

[22] Di Y., Wang X., Thomas A., Antonietti M.: 'Making metal_carbon nitride heterojunctions for improved photocatalytic hydrogen evolution with visible light', *ChemCatChem*, 2010, **2**, pp. 834–838

[23] Moon J., Yun C.Y., Chung K., Kang M., Yi J.: 'Photocatalytic activation of TiO_2 under visible light using Acid Red 44', *Catal. Today*, 2003, **87**, pp. 77–86

[24] Sehnert J., Baerwinkel K., Senker J.: 'Ab initio calculation of solid-state NMR spectra for different triazine and heptazine based structure proposals of g-C_3N_4', *J. Phys. Chem. B*, 2007, **111**, pp. 10671–10680

[25] Zhang Y., Liu J., Wu G., Chen W.: 'Porous graphitic carbon nitride synthesized via direct polymerization of urea for efficient sunlight-driven photocatalytic hydrogen production', *Nanoscale*, 2012, **4**, pp. 5300–5303